Liquid Crystals
Publication details, including instructions for authors and subscription information:
http://www.informaworld.com/smpp/title~content=t713926090

Memory effects in randomly perturbed systems exhibiting continuous symmetry breaking

M. Cvetko[ab]; M. Ambrožič[bc]; S. Kralj[bd]
[a] Regional Development Agency Mura Ltd, Lendavska 5a, 9000 Murska Sobota, Slovenia [b] Laboratory of Physics of Complex Systems, Faculty of Natural Sciences and Mathematics, University of Maribor, Koroška 160, 2000 Maribor, Slovenia [c] Engineering Ceramics Department, Jožef Stefan Institute, Jamova 39, 1000 Ljubljana, Slovenia [d] Condensed Matter Physics Department, Jožef Stefan Institute, Jamova 39, 1000 Ljubljana, Slovenia

To cite this Article Cvetko, M. , Ambrožič, M. and Kralj, S.(2009) 'Memory effects in randomly perturbed systems exhibiting continuous symmetry breaking', Liquid Crystals, 36: 1, 33 — 41
To link to this Article: DOI: 10.1080/02678290802638431
URL: http://dx.doi.org/10.1080/02678290802638431

Liquid Crystals,
Vol. 36, No. 1, January 2009, 33–41

Taylor & Francis
Taylor & Francis Group

Memory effects in randomly perturbed systems exhibiting continuous symmetry breaking

M. Cvetko[a,c]*, M. Ambrožič[b,c] and S. Kralj[c,d]

[a]*Regional Development Agency Mura Ltd, Lendavska 5a, 9000 Murska Sobota, Slovenia;* [b]*Engineering Ceramics Department, Jožef Stefan Institute, Jamova 39, 1000 Ljubljana, Slovenia;* [c]*Laboratory of Physics of Complex Systems, Faculty of Natural Sciences and Mathematics, University of Maribor, Koroška 160, 2000 Maribor, Slovenia;* [d]*Condensed Matter Physics Department, Jožef Stefan Institute, Jamova 39, 1000 Ljubljana, Slovenia*

We studied pattern characteristics in randomly perturbed structures exhibiting continuous symmetry breaking. A Lebwohl–Lasher-type lattice model was used which described well the onset of orientational ordering of a system of rod-like objects. For example, such systems mimic the orientational ordering tendency in liquid crystals or in an ensemble of nanotubes. We set impurities to impose a random anisotropy type of disorder on the objects. Structural characteristics were studied as a function of concentration of impurities, interaction strength w between impurities and rod-like objects, external ordering strength and history of samples. We showed that the characteristic linear size of patterns and range of ordering strongly depend on the history of samples for weak enough strength w. The two-dimensional and three-dimensional simulations yielded qualitatively similar results.

Keywords: memory effect; liquid crystals; nanotubes; structural order; percolation

1. Introduction

Domain patterns are commonly encountered in nature. They are formed in various condensed matter systems (e.g. in magnetic materials, liquid crystals) (*1, 2*), social systems and even in cosmology (*1*) (the domain-type pattern in the hypothetical Higgs field in the early universe (*3*)). The understanding of basic mechanisms driving and stabilising domain patterns is of interest in all branches of physics. Furthermore, details of such patterns strongly influence mechanical, electrical and optical (in transparent media) properties in various condensed matter systems. Therefore, such studies are also of great importance for several applications.

Domain-type patterns are unavoidable in phases or structures that are reached via a fast enough continuous symmetry breaking phase transition (*1*), and are the focus of our study. In practice such domains are often stabilised by various impurities. In order to illustrate basic mechanisms of domain patterning in such systems we first consider a temperature-driven phase transition from a paramagnetic to a ferromagnetic phase in a pure magnetic system. Above the phase transition temperature T_c the system exhibits continuous orientational symmetry (all orientations in the system are equivalent). Below the transition temperature, a homogeneously aligned structure along a single symmetry breaking direction represents an equilibrium configuration. However, in the case of a fast enough phase transition local fluctuations nucleate spatially different symmetry breaking directions. The resulting orientational frustration gives rise to domain-type ordering. Note that domains become visible (the so called protodomains) only when the degree of ordering is large enough. This happens roughly after the Zurek time (*1*) after the phase transition temperature was crossed. Studies in various condensed matter systems reveal that the size of the protodomains strongly depends on the quench rate τ_Q (*1*). The resulting domain pattern growth is well characterised by a single average domain length ξ_d (*1, 2*). In time, large domains grow at the expense of smaller ones. Soon after the transition, a scaling regime is entered in which the domain growth follows a power law (*2*) $\xi_d \propto t^{\gamma}$, where γ is a scaling coefficient.

The presence of impurities may hinder domain growth and stabilise the system into a domain-type pattern. One intuitively expects that this pattern would depend on the relative size $\xi_d^{(proto)}$ of an average protodomain and average separation of impurities. As $\xi_d^{(proto)} = \xi_d^{(proto)}(\tau_Q)$ we expect that kinetics significantly influence the saturated domain pattern. However, most studies so far in randomly perturbed systems were carried out based on static approaches. The majority assumed that impurities enforce a kind of quenched random-field disorder (*4–10*). The pioneering work by Imry and Ma (*4*) predicts the onset of a domain-type pattern characterised by a single length ξ_d obeying the scaling law $\xi_d \propto w^{\frac{-2}{(4-d)}}$. Here, w stands for the disorder strength and d is the space dimensionality. The resulting phase possesses short range order (SRO). However, several subsequent studies suggest that the quasi long range order (QLRO) is established (*5, 6*) instead.

*Corresponding author. Email: matej.cvetko@rra-mura.si

ISSN 0267-8292 print/ISSN 1366-5855 online

DOI: 10.1080/02678290802638431
http://www.informaworld.com

Lately many such studies were carried out in various randomly perturbed liquid crystals (LCs) (*7–10*). LCs (*11–13*) are especially adequate as a testing system due to their softness, liquid character, transparency and rich variety of different phases and structures exhibiting various physical phenomena. Consequently, samples can be relatively easily prepared and experimentally probed (*14*). As a source of random field-type disorder one conventionally uses: i) various porous matrices (*7*) serving as a host system for LCs; or ii) aerosol–LC mixtures (*7, 15*). In the latter case, disorder is imposed via fractal-like networks formed from aerosil particles. Lately it has been shown (*16*) that nematic LC-like ordering can be observed also in systems of nanotubes which are promising to revolutionise future technologies. Different structures of nanotubes, due to their inherent geometrical anisotropic properties, can yield remarkably different material properties. Consequently, several recent studies (*16–18*) have been devoted towards an understanding of the basic ordering mechanisms in such systems.

The aim of this paper is to demonstrate that the domain pattern in randomly perturbed systems strongly depends on the history of a sample. For this purpose we used a simple lattice model simulating an ensemble of nematic LC molecules (*7*) or nanotubes (*16–18*), which experience the random anisotropy field. We show that by changing the history of samples large quantitative and even qualitative changes could appear and that two-dimensional and three-dimensional simulation yield qualitatively similar results.

The plan of the paper is as follows. In Section 2, we introduce the Lebwohl–Lasher-type lattice model that we used. We consider the two- and three-dimensional cases in order to test the dimensionality dependence and robustness of results. In Section 3, we present the results. Conclusions are given in the last section. Some calculation details are presented in the Appendix.

2. Model

We consider an ensemble of $N=N_0^d$ cylindrically symmetrical particles within a lattice, where d stands for the dimensionality of the system. Neighbouring sites are separated for a distance a_0 in a cubic cell of length $L=N_0a_0$. Local orientational ordering of a particle at the ith site is given by a unit vector $\boldsymbol{S}_i$, to which we henceforth refer as the 'director'. We further set at randomly chosen sites of concentration p cylindrically symmetric quenched impurities enforcing orientational ordering along $\boldsymbol{e}_i$. The orientations of impurities were randomly chosen without any preferred global orientation. We also imposed an homogeneous external (e.g. electric or magnetic) ordering field $\boldsymbol{B}=B\boldsymbol{e}_B$, which enforces orientational ordering along $\boldsymbol{e}_B$. We considered systems exhibiting the so-called head-to-tail invariance, where $\pm\boldsymbol{S}_i$ orientations are equivalent. This is characteristic for most LC molecules (where several structural details are averaged out via relatively fast molecular rotations) or nanotubes. With this in mind, we expressed the interaction energy of the system as (*7, 19, 20*)

$$W=-\frac{J}{2}\sum_{i,j}\left(\boldsymbol{S}_i\cdot\boldsymbol{S}_j\right)^2-\sum_i w_i(\boldsymbol{S}_i\cdot\boldsymbol{e}_i)^2-B^2\sum_i(\boldsymbol{S}_i\cdot\boldsymbol{e}_B)^2. \tag{1}$$

Here, $J>0$ describes the ordering interaction among neighbouring molecules tending to orient directors parallel or antiparallel. The sum over indices i runs over all the particles, and the indices j run over the first neighbours of the ith particle. At randomly chosen sites of concentration p, we placed impurities which are coupled with surrounding directors by the random anisotropy-type interaction (*21*) of anchoring strength $w_i=w>0$. At the remaining sites, we set $w_i=0$. Our interest was to find the main structural characteristic of $\boldsymbol{S}_i$ patterns as a function of p, w and a history of such systems.

We described ordering in the three dimensional ($d=3$) Cartesian coordinate frame (x, y, z), whose axes point along unit vectors $\boldsymbol{e}_x$, $\boldsymbol{e}_y$ and $\boldsymbol{e}_z$, respectively. The external field is oriented along the x-axis, i.e. $\boldsymbol{e}_B=\boldsymbol{e}_x$. We considered behaviour in two and three dimensions, to which we henceforth refer to as the 2D and 3D model, respectively. In the 2D case, where directors are constrained to the (x, y) plane, we parameterise $\boldsymbol{S}_i$ as

$$\boldsymbol{S}_i=\boldsymbol{e}_x\cos\theta_i+\boldsymbol{e}_y\sin\theta_i. \tag{2}$$

In the 3D model we parameterise unit vectors $\mathbf{S}_i$ as

$$\boldsymbol{S}_i=\boldsymbol{e}_xS_x^{(i)}+\boldsymbol{e}_yS_y^{(i)}+\boldsymbol{e}_zS_z^{(i)}. \tag{3}$$

For latter convenience we scale quantities in Equation (1) with respect to J: $\tilde{\boldsymbol{W}}=W/J$, $\tilde{w}_i=w_i/J$, $\tilde{\boldsymbol{B}}=B/\sqrt{J}$. We henceforth omit the tildes.

In the 2D model the total energy W of the configuration $N=N_0^2$ directors is minimised with respect to the angles θ_i, yielding the set of N equilibrium equations. In the 3D model we minimise W over $S_x^{(i)}$, $S_y^{(i)}$, $S_z^{(i)}$ taking into account the constraint $S_x^{(i)2}+S_y^{(i)2}+S_z^{(i)2}=1$ (i.e. $|\boldsymbol{S}_i|=1$). Therefore, we neglect the role of thermal fluctuations

and consider configurations at zero temperature. In case of nematic ordering in LCs such an assumption is sensible deep in the nematic phase (i.e. well below the isotropic-nematic LC phase transition temperature).

The equilibrium equations and calculation details are summarised in Appendix 1. At cell boundaries, we imposed the periodic boundary conditions.

In simulations we either originated from randomly distributed orientations of directors, or from homogeneously aligned samples along a symmetry breaking direction. In the latter case, the directors are initially homogeneously aligned along $\boldsymbol{e}_x$. We henceforth refer to these cases as the i) random and ii) homogeneous case, respectively. The random case can be experimentally realised by quenching the system from the isotropic phase to the ordered phase without an external field (i.e. $B=0$). This can be achieved either via a sudden decrease of temperature or sudden increase of pressure. The homogeneous case can be realised by applying first a strong homogeneous external field $\boldsymbol{B}$ along a symmetry breaking direction. After a well enough alignment is achieved, the field is switched off.

In order to diminish the influence of statistical variations we carried out several simulations (typically $N_{rep}\sim10$) for a given set of parameters (i.e. w, p and a chosen initial condition).

From obtained configurations of directors we calculated the orientational correlation function $G(r)$. It measures orientational correlation of directors as a function of their mutual separation r. We define it as

$$G(r)=\langle 2\left(\boldsymbol{S}_i\cdot\boldsymbol{S}_j\right)^2-1\rangle, \tag{4}$$

$$G(r)=\frac{1}{2}\langle 3\left(\boldsymbol{S}_i\cdot\boldsymbol{S}_j\right)^2-1\rangle \tag{5}$$

in 2D (Equation (4)) and 3D (Equation (5)) space. The brackets <…> denote the average over all lattice sites that are separated for a distance r. If the directors are completely correlated (i.e. homogeneously aligned along a symmetry breaking direction), it follows $G(r)=1$. On the other hand, $G(r)=0$ reflects completely uncorrelated directors. Since each director is parallel with itself, it holds that $G(0)=1$. The correlation function is a decreasing function of the distance r. We performed several tests to verify the isotropic character of $G(r)$, i.e. $G(r)=\mathrm{G}(\boldsymbol{r})$.

In order to obtain structural details from a calculated $G(r)$ dependence we fit it with the ansatz

$$G(r)=(1-s)e^{-(r/\xi)^m}+s, \tag{6}$$

where the ξ, m, and s are adjustable parameters. In simulations distances are scaled with respect to a_0 (the nearest neighbour distance). The quantity ξ estimates the average domain length (the coherence length) of the system. Over this length the directors are relatively well correlated. The distribution width of ξ values is measured by m. Dominance of a single coherence length in the system is signalled by $m\sim1$. A magnitude and system size dependence of s reveals the degree of ordering within the system (*22*). The case $s=0$ indicates the SRO. A finite value of s reveals either the long range order (LRO) or QLRO. To distinguish between these two cases a finite size analysis $s(N_0)$ must be carried out. If $s(N_0)$ saturates at a finite value the system exhibits LRO. If $s(N_0)$ dependence exhibits algebraic dependence on N_0 the system possesses QLRO (*5*).

3. Results

We studied the structure of systems as a function of impurity site-occupation probability P, anchoring strength w between directors, external field strength B and history of the system. In the first subsection we consider the percolation properties of impurities in 2D and 3D space. In the second part we analyse structural characteristics as various parameters are varied above and below the percolation threshold. This is followed by an analysis of external ordering field-induced memory effects.

3.1. Percolation

It is expected that systems might show qualitatively different behaviour above and below the percolation threshold $p=p_c$ of impurities. For this reason we first analysed the percolation behaviour of 2D and 3D systems for typical cell dimensions implemented in our simulations.

On increasing the concentration p of impurities a percolation threshold is reached at $p=p_c$. This is well manifested in the $P(p)$ dependence shown in Figure 1, where P stands for the probability that there exists a connected path of impurity sites between the bottom and upper (or left and right) side of the simulation cell. In the thermodynamic limit $N\rightarrow\infty$ the $P(p)$ dependence displays a phase transition type of behaviour, where P plays the role of order parameter, i.e. $P(p>p_c)>0$ and $P(p<p_c)=0$. For a finite simulation cell a pretransitional tail appears below p_c, and at $p\sim p_c$ the $P(p)$ steepness decreases with decreasing N. For 2D and 3D cases, the $P(p)$ dependencies show qualitatively similar behaviour, where $p_c(2\mathrm{D})\sim0.59$ and $p_c(3\mathrm{D})\sim0.30$. A typical percolated pattern in 2D is shown in Figure 2. In simulations we use large enough values of N_0, so that finite size effects are negligible.

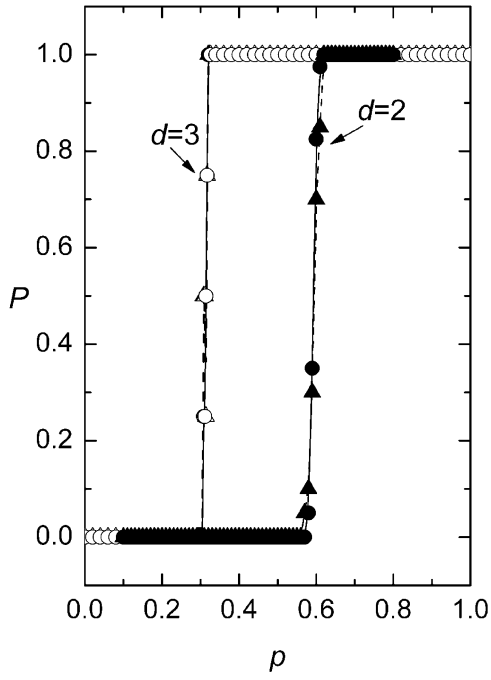

Figure 1. The percolation probability P as a function of p and system size $N = N_0^d$ for $d=2$ and $d=3$. For a finite value of N the percolation threshold ($p=p_c$) is defined as the point where $P=0.5$. For $d=2$ and $d=3$ we obtain $p_c \sim 0.59$ and $p_c \sim 0.30$, respectively, roughly irrespective of the system size. (Δ) $N_0=60$; (○) $N_0=80$; (▲) $N_0=150$; (●) $N_0=260$.

3.2. *Structural properties*

In Figure 3 typical correlation functions $G(r)$ for $p<p_c$ and $p>p_c$ are plotted for the random and homogeneous initial conditions. Both 2D (Figure 3(a)) and 3D (Figure 3(b)) cells were studied. It can be seen that in the random case correlations vanish for $r \gg \xi$ (i.e. $s=0$), which is characteristic for SRO. On the contrary $G(r)$ dependencies obtained from the homogeneous initial condition yield $s>0$.

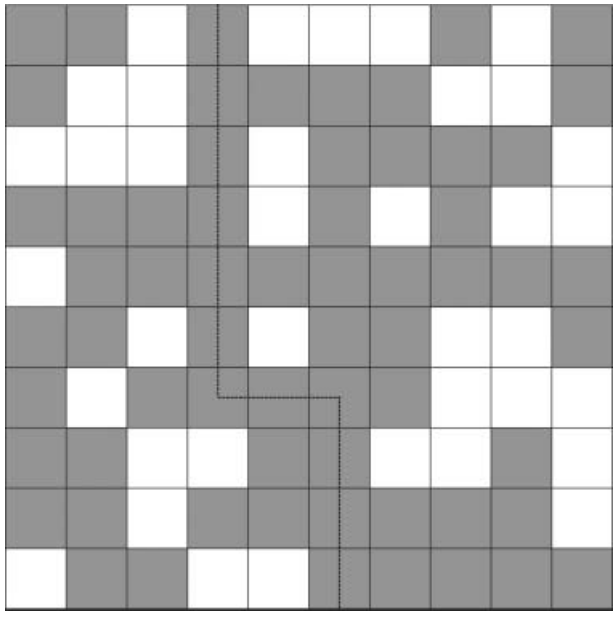

Figure 2. A schematic view of a 2D simulation cell with $N_0=10$, where the darker areas in the lattice represent areas occupied by impurities. Dashed line shows a possible percolation path.

More structural details as p is varied for a relatively weak anchoring ($w=1$) are given in Figure 4 for 2D and 3D systems. By fitting simulation results with Equation (6), we obtained $\xi(p)$, $m(p)$ and $s(p)$ dependencies that are shown in Figure 4. One of the key results of the study is that values of ξ strongly depend (Figure 4(a)) on the history of systems for a weak enough anchoring strength w. A typical domain size is larger if one originates from the homogeneous initial configuration. We obtained a scaling relation between ξ and p, which is again history dependent. We obtain $\xi \propto p^{-0.533 \pm 0.003}$ (2D), $\xi \propto p^{-0.92 \pm 0.03}$ (3D) for the homogeneous case and $\xi \propto p^{-0.359 \pm 0.005}$ (2D), $\xi \propto p^{-0.95 \pm 0.02}$ (3D) for the random case.

Information on the distribution of domain coherence lengths about their mean value ξ is given in Figure 4(b) where $m(p)$ is plotted. For the homogeneous case we obtained $m \sim 1.18$ (2D), $m \sim 0.95$ (3D), and for the random case $m \sim 1.39$ (2D), $m \sim 1.17$ (3D). A larger value of m for the random case signals broader distribution of domain coherence length values in comparison with the homogeneous case. The simulations did not reveal any systematic changes in m as p is varied. Note that values of m are strongly scattered because structural details of $G(r)$ are relatively weakly m-dependent.

In Figure 4(c) $s(p)$ is plotted. In the random case we obtained $s=0$ for any p. Therefore, if starting from isotropically distributed orientations of $\mathbf{S}_i$, then final configurations exhibit SRO. In the homogeneous case s gradually decreased with p, but remained finite for the chosen anchoring strength ($w=1$ for 2D and $w=3$ for 3D systems).

Finite size analysis for two concentrations was carried out, which is shown in Figure 5. It can be seen that $s(N_0)$ dependencies saturate at a finite value of s, which is a signature of LRO. We carried out simulations up to values $N_0=400$ for $d=2$ and $N_0=140$ for $d=3$.

Note that for larger anchoring values LRO order for structures obtained from the homogeneous initial configuration can be replaced by QLRO or even SRO. In order to demonstrate that we studied structural changes on increasing w starting from the weak anchoring regime $w=1$. In Figure 6, $s(p)$ is plotted for different anchoring strengths w for the homogeneous case. It can be seen that a SRO can be obtained above a certain threshold value of w above a critical value p_w of

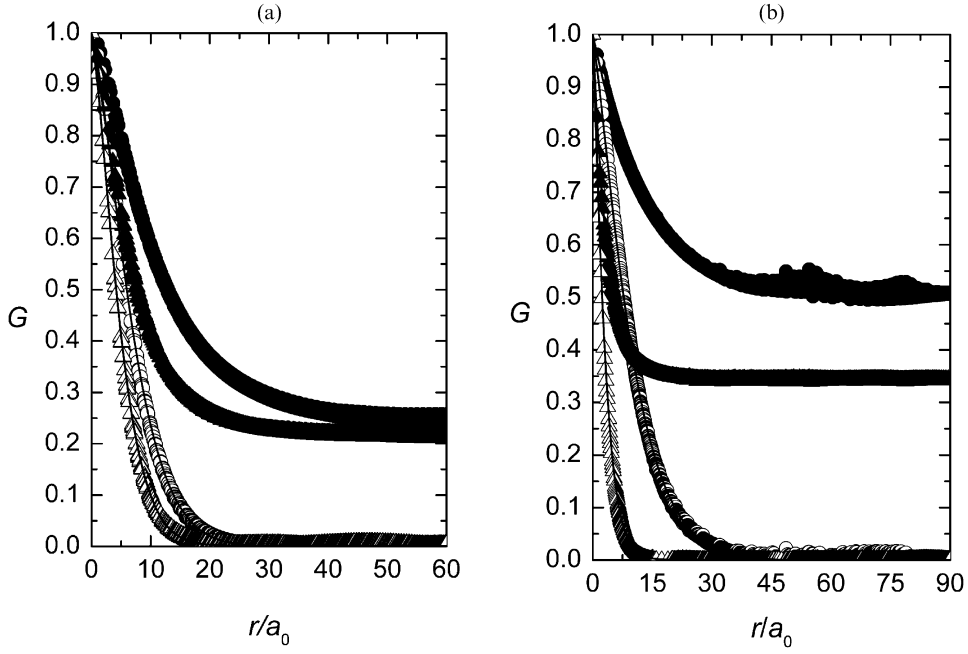

Figures 3. $G(r)$ for $p>p_c$ and $p<p_c$ for the homogeneous and random case, $B=0$. (a) $d=2$, $w=1$, $p_c\sim0.59$, $N_0=260$. (●) $p=0.3$, homogeneous; (▲) $p=0.7$, homogeneous; (○) $p=0.3$, random; (Δ) $p=0.7$, random. (b) $d=3$, $w=3$, $p_c\sim0.30$, $N_0=80$. (●) $p=0.2$, homogeneous; (▲) $p=0.7$, homogeneous; (○) $p=0.2$, random; (Δ) $p=0.7$, random.

impurity concentration. The value of p_w decreases with increasing w. For example, for $w=5$ and $w=\infty$ the SRO is realised above $p_w\sim0.8$ and $p_w\sim0.6$, respectively.

Note that apparent changes on crossing the percolation threshold on increasing p were noticed.

3.3. *Field induced memory effects*

We further analysed how the domain-type ordering could be manipulated with external magnetic or electric ordering field. For this purpose we originated from the random initial configuration. We then applied an external field of strength B and calculated the configuration for different concentrations of impurities. Then the field was switched off and the configuration calculated again, to which we henceforth refer as the 'switch-off configuration'. The corresponding calculated s and ξ behaviour is shown in Figures 7 and 8 for 2D (a) and 3D (b) space.

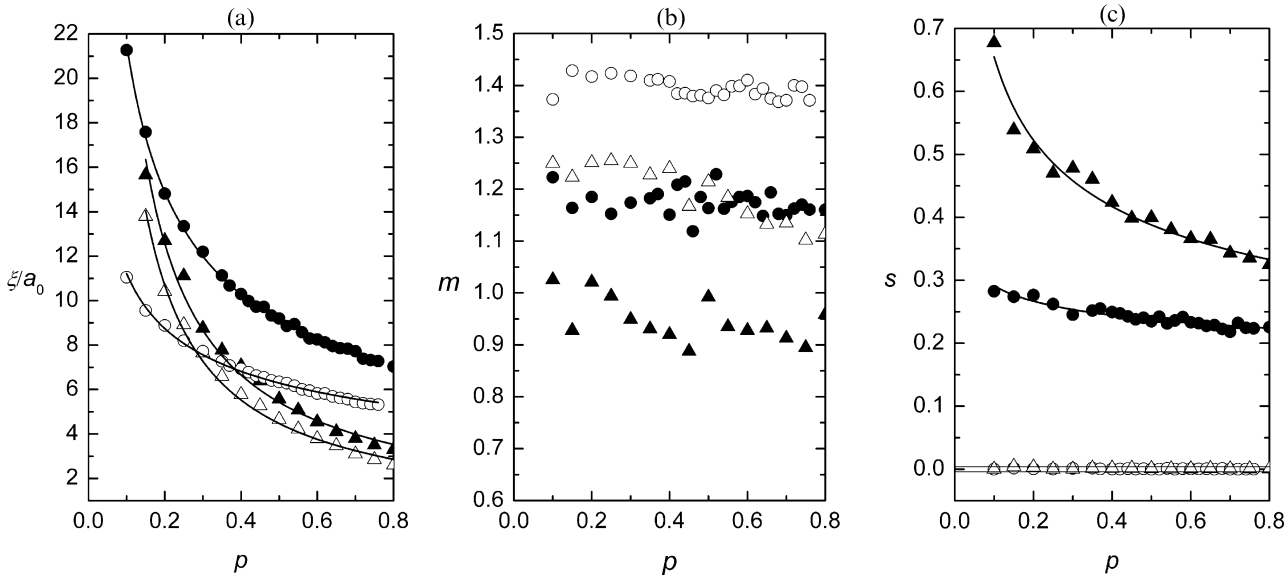

Figures 4. Structural characteristics as p is varied for $B=0$, $w=1$ for 2D and $w=3$ for 3D system. (a) $\xi(p)$, (b) $m(p)$, (c) $s(p)$. (●) homogeneous, 2D; (○) random, 2D; (▲) homogeneous, 3D; (Δ) random, 3D. Lines denote the fits.

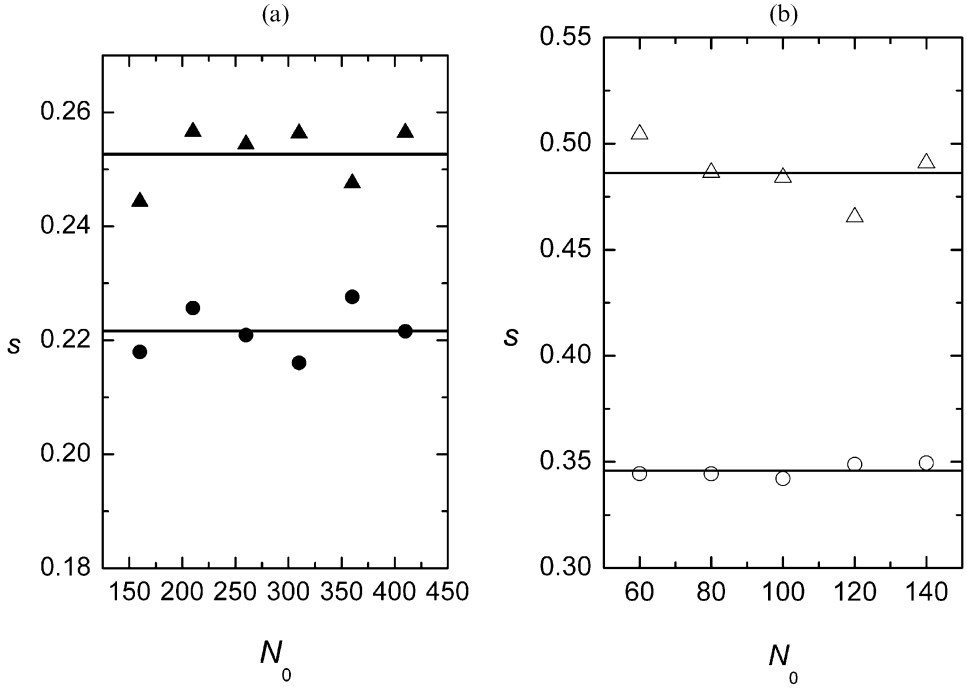

Figures 5. Finite size analysis $s(N_0)$ for $p<p_c$ and $p>p_c$ for the homogeneous case; $B=0$ (a) $w=1$ for the 2D system, (▲) $p=0.3$; (●) $p=0.7$ and (b) $w=3$ for the 3D system, (Δ) $p=0.2$; (○) $p=0.7$. Lines denote average values.

Dashed lines mark the values of observables in the presence of a field of strength B, while full lines mark values after the field was switched off. From Figure 7 it can be seen that the presence of external field develops QLRO or LRO (time-consuming finite size analysis to distinguish between the two cases was not carried out). This range of ordering remained as the field was switched off, although the correlation strength was reduced. Note that above a certain field strength the degree of ordering in the switch-off configuration is saturated, i.e. becomes independent of B. Both 2D and 3D cases showed qualitatively similar behaviour for all concentrations studied (i.e. for $p \in [0.25, 0.75]$).

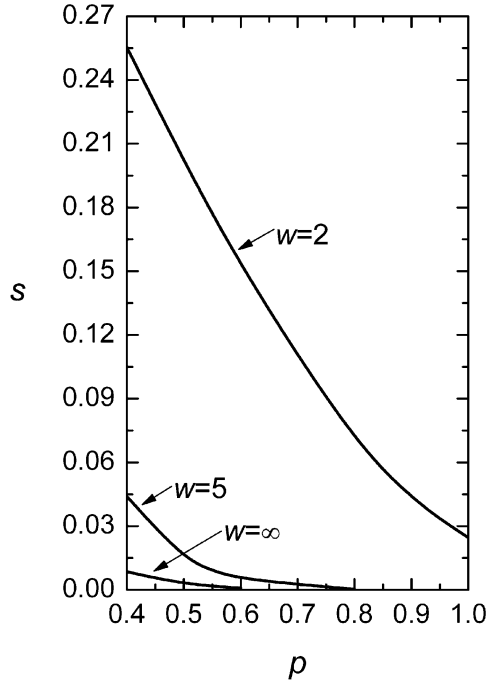

Figure 6. $s(p)$ for different anchoring strengths w for the homogeneous 2D case, $N_0=250$.

The corresponding changes in ξ are shown in Figure 8. With increasing B the ξ values for samples with different p decrease and converge to the same value, which is equal to the external field coherence length. In the switched-off configuration the average domain coherence length increases and again for a large enough value of B saturates at a fixed value.

4. Conclusions

We studied the typical domain size ξ and configuration character of a randomly perturbed system exhibiting continuous symmetry breaking. As a model system we used rod-like objects within a cubic lattice interacting via a Lebwohl–Lasher-type interaction. The structure of the system is described in terms of the director field $\boldsymbol{S}_i$, where the unit vector $\boldsymbol{S}$ exhibits head-to-tile invariance. An example of such systems represents LC molecules or nanotubes. We further introduced impurities of concentration p, which impose the so-called random anisotropy field

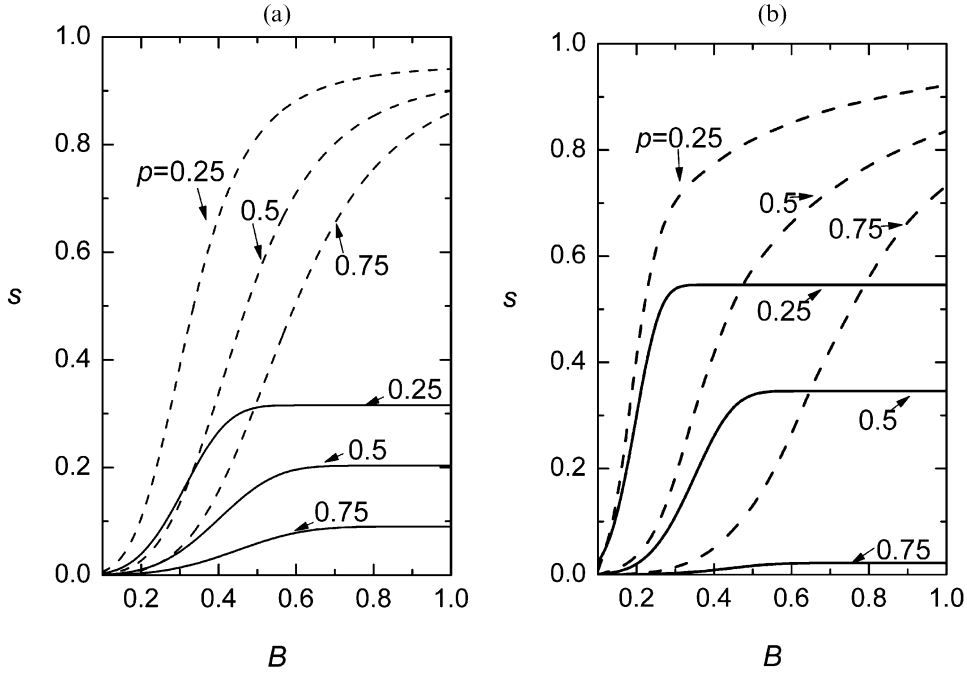

Figure 7. $s(B)$ for (a) $d=2$, $w=2$, $N_0=250$ and (b) $d=3$, $w=4$, $N_0=60$; random case. Dashed curves: configurations calculated in the presence of external field B. Full curves: configurations calculated after the field was switched off.

disorder to directors. We studied the domain-type pattern of molecules as a function of p, anchoring strength w between a neighbouring director and impurity, and history of samples. In simulations we quenched the directors either from the random or homogeneous initial configuration.

Our results indicated that a history of system strongly influences: i) the average domain coherence

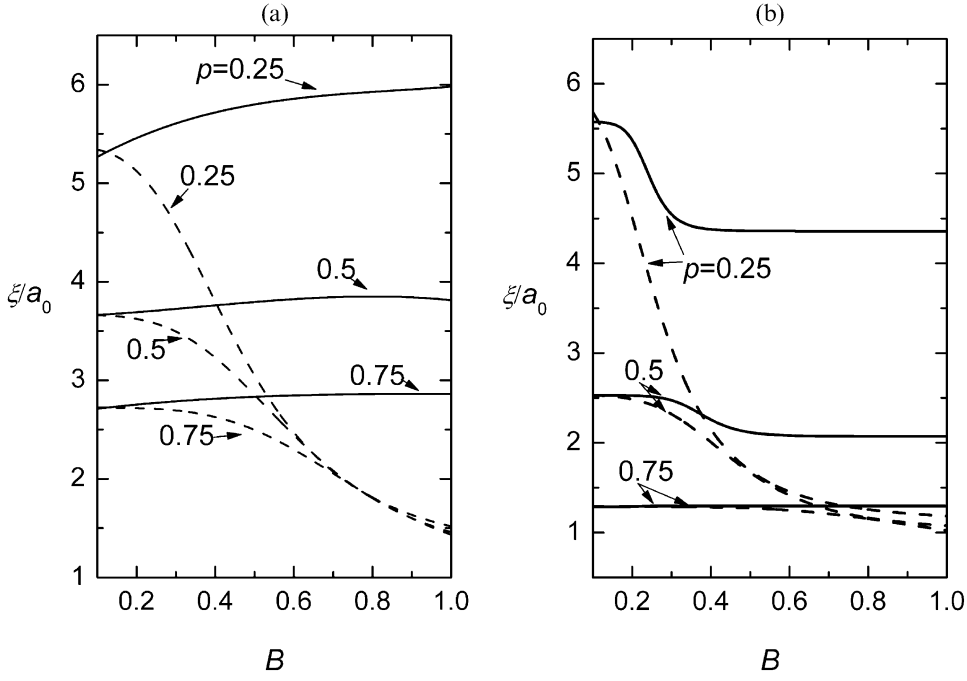

Figure 8. $\xi(B)$ for (a) $d=2$, $w=2$, $N_0=250$ and (b) $d=3$, $w=4$, $N_0=60$; random case. Dashed curves: configurations calculated in the presence of external field B. Full curves: configurations calculated after the field was switched off.

length; and ii) the range of ordering in the system. In the random case the obtained order is always short ranged. On the contrary, in the homogeneous case, SRO is obtained only for strong enough anchoring and large enough concentration p. In other cases, the ordering is either QLRO or LRO. For example, we obtained LRO for $w=1$ for all concentrations of impurities. We did not observe any apparent changes above and below the threshold. We further studied memory effects for the random initial configuration. With increasing external ordering field B either QLRO or LRO is realised. This ordering is preserved even if the field is switched off. In addition the average coherence length ξ is larger in comparison to the 'virgin' configuration which was not exposed to B. The degree of remanent global ordering in the switch-off configuration becomes saturated for a large enough value of B. Therefore, one can control the degree of global ordering and average domain coherence size by temporarily exposing a system to an external ordering field. Our simulations further showed that in such cases 2D and 3D systems exhibit qualitatively similar behaviour.

Acknowledgments

Matej Cvetko acknowledges the support of the EU European Social Fund. Research is performed within the Operative Programme for the Development of Human Resources for the period 2007–13. Milan Ambrozic and Samo Kralj acknowledge support from the Slovenian Research Agency (Grant J1–0155).

References

(1) Zurek W.H. *Nature* **1985**, *317*, 505.
(2) Bray A.J. *Adv. Phys.* **1994**, *43*, 357.
(3) Kibble T.W.B. *J. Phys. A: Math.Gen.* **1976**, *9*, 1387.
(4) Imry Y.; Ma S. *Phys. Rev. Lett.* **1975**, *35*, 1399.
(5) Feldman D.E. *Phys. Rev. Lett.* **2000**, *85*, 4886.
(6) Chakrabarti J. *Phys. Rev. Lett.* **1998**, *81*, 385.
(7) Cleaver D.J.; Kralj S.; Sluckin T.J.; Allen M P., In *Liquid Crystals in Complex Geometries Formed by Polymer and Porous Networks*, Crawford G.P. and Zumer S. Eds.; Oxford University Press: London, 1996.
(8) Radzihovsky L.; Toner J. *Phys. Rev. Lett.* **1997**, *79*, 4214.
(9) Popa-Nita V. *Eur. Phys. J.* **1999**, *83*, 12.
(10) Popa-Nita V.; Romano S. *Chem. Phys.* **2001**, *91*, 264.
(11) de Gennes P.G.; Prost J. *The Physics of Liquid Crystals*; Oxford University Press: Oxford, 1993.
(12) Virga E.G. *Variational Theories for Liquid Crystals*; Chapman Hall: London, 1994.
(13) Kleman M.; Lavrentovich O.D. *Soft Matter Physics*; Springer-Verlag: Berlin, 2002.
(14) Kurik M.V.; Lavrentovich O.D. *Usp. Fiziol. Nauk* **1988**, *154*, 381.
(15) Sinha G.; Leys J.; Glorieux C.; Thoen J. *Phys. Rev.* E **2005**, *72*, 051710.
(16) Lagerwall J.; Scalia G.; Haluska M.; Dettlar-Weglikowska U.; Roth S.; Giesselmann F. *Adv. Mater.* **2007**, *19*, 359.
(17) Lynch N.D.; Patrick L.D. *Nano Lett.* **2002**, *2*, 1197.
(18) Jiann K.; Hurt R.H.; Sheldon B.W.; Crawford G.P. *Appl. Phys. Lett.* **2006**, *88*, 163110.
(19) Lebwohl P.A.; Lasher G. *Phys. Rev.* A **1972**, *6*, 426.
(20) Romano S. *Int. J. Mod. Phys* B **2002**, *16*, 2901, (and references therein).
(21) Harris R.; Plischke M.; Zuckerman M.J. *Phys. Rev. Lett.* **1973**, *31*, 160.
(22) Giamarchi T.; Doussal P.L. *Phys. Rev.* B **1995**, *52*, 1242.

Appendix 1. Numerical approach

2D case.

The unit director field in the two-dimensional (2D) model is characterised by angles θ_{ij} with respect to the x-axis:

$$\boldsymbol{S}_{ij} = \boldsymbol{e}_x \cos\theta_{ij} + \boldsymbol{e}_y \sin\theta_{ij}, \tag{A1}$$

where $1 \leqslant i \leqslant N_0$ and $1 \leqslant j \leqslant N_0$. The director is coupled to its four nearest neighbours. In addition it may be influenced by an impurity at the same site and by the homogeneous external field $\boldsymbol{B}=B\boldsymbol{e}_x$. We further scale the total interaction energy W with respect to the coupling constant J. It follows that

$$\begin{aligned}\tilde{W} &= \frac{W}{J} \\ &= -\frac{1}{2}\sum_{i,j}\begin{pmatrix}\cos^2(\theta_{i+1,j}-\theta_{ij}) \\ +\cos^2(\theta_{i-1,j}-\theta_{ij}) \\ +\cos^2(\theta_{i,j+1}-\theta_{ij}) \\ +\cos^2(\theta_{i,j-1}-\theta_{ij})\end{pmatrix} \\ &\quad -\tilde{w}\sum_{i,j} p_{ij}\cos^2\left(\theta_{ij}^{(ran)}-\theta_{ij}\right) - \tilde{\boldsymbol{B}}^2\sum_{i,j}\cos^2\theta_{ij}.\end{aligned} \tag{A2}$$

Here $\tilde{w}=w/J$, $\tilde{\boldsymbol{B}}=\boldsymbol{B}/\sqrt{J}$, and we henceforth skip the tildes. The angles $\theta_{ij}^{(ran)}$ in the w-term are random preferential angles at the sites with impurities calculated via the random-number generator. The presence/absence of an impurity in each cell is also determined by the random-number generator. The coefficient p_{ij} takes the value 1 or 0, denoting the presence or absence of an impurity at the ijth site. The total interaction energy is minimised with respect to all N_0^2 angles θ_{ij} and the corresponding equilibrium equations are solved numerically. Periodic boundary conditions have been adopted. The director at the right boundary $(S_{N_0 j})$ feels the director at the opposite face (S_{1j}) as its right nearest neighbour, and similarly for other boundaries. In order to diminish the influence of statistical variations we repeat several ($N_{rep}\sim 10$ or

more) times the initial setup of random impurities and director relaxation followed by averaging the corresponding correlation functions.

3D case.

The three-dimensional (3D) system consists of a lattice of $N_0 \times N_0 \times N_0$ sites with unit directors

$$\boldsymbol{S}_{ijk} = \boldsymbol{e}_x S_x^{(ijk)} + \boldsymbol{e}_y S_y^{(ijk)} + \boldsymbol{e}_z S_z^{(ijk)}. \tag{A3}$$

In contrast to the 2D problem, we found that the use of conventional polar angles to characterise the director field results in some troubles and inconsistencies of the numerical relaxation method, such as convergence problems, and numerical preference of one coordinate axis, although the system should behave isotropically. In order to circumvent such problems direct mathematical operations on Cartesian director components have been performed.

We express the total interaction energy functional as $W = \sum_{ijk} W_{ijk}$ where the term W_{ijk} consists of three parts:

$$W_{ijk} = -\frac{1}{2}\sum_{i'} \left(\boldsymbol{S}_{ijk}\cdot\boldsymbol{S}_{i'}\right)^2 - wp_{ijk}\left(\boldsymbol{S}_{ijk}\cdot\boldsymbol{e}_{ijk}{}^{(ran)}\right)^2 - B^2\left(\boldsymbol{S}_{ijk}\cdot\boldsymbol{e}_x\right)^2. \tag{A4}$$

The total interaction energy is normalised as in the 2D case by setting $J=1$. The indices i', j', k' run over the first neighbours of the point described by the indices i, j, k. The quantity p_{ijk} in the second term is 1 if the site contains an impurity, and 0 otherwise, while the unit vector $\boldsymbol{e}_{ijk}^{(ran)}$ describes the random preferential orientation enforced by the impurity at the site labelled by the indices i, j, k.

The equilibrium director configuration is obtained by minimising the total interaction energy with respect to all the directors by taking into account the normalisation condition $\boldsymbol{S}_{ijk}^2 = 1$. The resulting potential to be mimimised reads $W^* = \sum_{ijk} W_{ijk}{}^*$,where

$$W_{ijk}{}^* = \lambda_{ijk}\left(S_{ijk}{}^2 - 1\right) + W_{ijk}, \tag{A5}$$

and λ_{ijk} are Lagrange multipliers. We minimise the potential W^* and obtain the following set of N_0^3 equations which are solved numerically:

$$\sum_{i'} \boldsymbol{g}\left(\boldsymbol{S}_{ijk}, \boldsymbol{S}_{i'}\right) + wp_{ijk}\boldsymbol{g}\left(\boldsymbol{S}_{ijk}, \boldsymbol{e}_{ijk}^{(ran)}\right) + B^2\boldsymbol{g}\left(\boldsymbol{S}_{ijk}, \boldsymbol{e}_x\right) = 0, \tag{A6}$$

where the vector function $\boldsymbol{g}$ is defined as

$$\boldsymbol{g}(\boldsymbol{v}_1, \boldsymbol{v}_2) = (\boldsymbol{v}_1\cdot\boldsymbol{v}_2)[\boldsymbol{v}_2 - (\boldsymbol{v}_1\cdot\boldsymbol{v}_2)\boldsymbol{v}_1]. \tag{A7}$$

The system of Equations (A6) is solved by the relaxation method which has been proved fast and reliable. Other aspects, for example, impurities setup, initial director configuration, boundary condition, etc., have been considered similarly as in the 2D case. Of course, instead of using the orientational angles θ_{ij}, Equations (A6) may be directly applied to the 2D problem simply by reducing the dimensionality by 1. Such tests showed the consistency of both approaches in 2D. Note that similar behaviour was observed in random magnets.